Cellulose (2016) 23:2597–2607
DOI 10.1007/s10570-016-0966-2

ORIGINAL PAPER

Pyrolyzed bacterial cellulose-supported SnO_2 nanocomposites as high-capacity anode materials for sodium-ion batteries

Burcu Dursun · Taner Sar · Ali Ata · Mathieu Morcrette · Meltem Yesilcimen Akbas · Rezan Demir-Cakan

Received: 18 January 2016 / Accepted: 18 May 2016 / Published online: 3 June 2016

Abstract Room-temperature sodium-based batteries have the potential for meeting large-scale grid energy storage needs. Inspired by the advancement of the design and building of electrode materials in lithium ion batteries, improved nano-architectured electrodes can be created for sodium-ion batteries, allowing increased electron transport kinetics and conductivities. Here, nanocomposites with 3D porous structures are reported as a high-capacity anode material for sodium-ion batteries by using an easy, low-cost and environmentally friendly synthesis of pyrolyzed bacterial celluloses (PBCs). Bacterial celluloses (BCs) produced by the *Gluconacetobacter xylinus* strain are pyrolyzed at 500, 750 and 1000 °C, resulting 50, 130 and 110 mAh g^{-1} capacities over 80 numbers of cycles, respectively, in the presence of the binary ethylene carbonate–propylene carbonate mixture. In order to increase the cell performances, in situ coated SnO_2 nanoparticles with bacterial cellulose (SnO_2@PBC) are produced by addition as synthesized 5-nm-sized SnO_2 nanoparticles into the BC growth medium together with the *G. xylinus* strain. Following the pyrolysis at 500 °C, the SnO_2@PBC composite is better able to handle the accommodation of the dramatic volume change of the incorporated SnO_2 nanoparticles because of the interaction of oxygen-containing moieties of bacterial cellulose nanofibrils with the SnO_2 nanoparticles during cellulose production. The resulting SnO_2@PBC composite presents highly stable capacity retention of around 400 mAh g^{-1} capacities at C/10 current density over 50 numbers of cycles.

Keywords Pyrolyzed bacterial cellulose · Carbon · SnO_2 · Anode · Sodium-ion batteries

Electronic supplementary material The online version of this article (doi:10.1007/s10570-016-0966-2) contains supplementary material, which is available to authorized users.

B. Dursun · A. Ata
Department of Material Science and Engineering, Gebze Technical University, 41400 Gebze, Turkey

T. Sar · M. Y. Akbas
Department of Molecular Biology and Genetics, Gebze Technical University, 41400 Gebze, Turkey

M. Y. Akbas (✉)
Institute of Biotechnology, Gebze Technical University, 41400 Gebze, Turkey
e-mail: akbasm@gtu.edu.tr

M. Morcrette
Laboratoire de Réactivité et Chimie des Solides, CNRS UMR 7314, Université de Picardie Jules Verne, 80039 Amiens, France

R. Demir-Cakan (✉)
Department of Chemical Engineering, Gebze Technical University, 41400 Gebze, Turkey
e-mail: demir-cakan@gtu.edu.tr

Introduction

Extensive use of renewable energy sources necessitates the development of low-cost and efficient energy storage systems. To address these needs, Li-ion battery systems (LIBs) have been extensively exploited in the last 3 decades. However, as the use of large-format Li batteries becomes widespread, the cost of the Li raw material has roughly doubled from the first application in 1991 to the present (Kim et al. 2012). Based on the wide availability, non-toxicity and low cost of sodium, ambient temperature sodium-based batteries have the potential for meeting large-scale grid energy storage needs.

Sodium-ion batteries (NIBs) have a working mechanism similar to that of LIBs. However, since the ionic radii of sodium and lithium are different, dissimilar thermodynamic and kinetic properties are expected between the individual cells. For instance, graphite, which is a commonly used anode material in Li-ion batteries, is considered nearly impossible for the application of NIBs since the ionic volume of sodium ions is almost double those of Li^+ ions resulting in difficulties to intercalate between the interlayer of graphite ($\sim$0.34 nm) (Cao et al. 2012; Falco et al. 2013; Komaba et al. 2003; Palomares et al. 2012; Sangster 2007; Slater et al. 2013). This limitation can be circumvented by sodium ion co-intercalation into graphite by using diglyme as an electrolyte solvent (Jache and Adelhelm 2014).

In recent years, different types of materials including carbonaceous materials, sodium alloys and metal oxides have been investigated as anodes for NIBs. The electrochemical insertion of sodium ions into carbon was first reported by Doeff et al. (Kubo et al. 2013) with a reversible capacity of $\sim$85 mAh g^{-1}. Disordered carbons including both hard and amorphous carbon are considered the dominant candidate materials for NIBs (Alcántara et al. 2005; Antonietti et al. 2007a, b; Cao et al. 2012; Komaba et al. 2011b; Kubo et al. 2013; Ponrouch et al. 2013; Soorholtz et al. 2013; Stevens and Dahn 2001; Tang et al. 2012; Wenzel et al. 2011; Xia and Dahn 2012; Zhao et al. 2013) because of the larger interlayer space between the graphene sheets. Stevens and Dahn reported the reversible sodium capacities of hard carbons derived from sugars achieving 300 mAh g^{-1} (Soorholtz et al. 2013). Tang et al. (2012) have also demonstrated the use of hollow carbon nanospheres as high rate anode materials for NIBs.

Although most studies focus on hard carbon materials for NIBs because of their large interlayer distance, alternative oxide anodes such as $Na_2Ti_3O_7$ (Senguttuvan et al. 2011), $Na_2C_8H_4O_4$ (Zhao et al. 2013) and amorphous TiO_2 (Xiong et al. 2011) nanotubes have also been investigated. However, the capacities of these materials toward sodium storage are still low. Tin dioxide (SnO_2) is a promising anode material in LIBs because of its high theoretical capacity, although it suffers from an extremely large volume change during charge and discharge resulting in electrode degradation and fast capacity fading (Sevilla et al. 2012; Yu et al. 2013). SnO_2 can exhibit a theoretical reversible specific capacity of 667 mAh g^{-1} (Park et al. 2014; Wang et al. 2013b, 2014). Wang's group reported a SnO_2@graphene nanocomposite demonstrating a capacity of about 302 mAh g^{-1} at 160 mA g^{-1} (Su et al. 2013). Wang's group also reported the SnO_2@MWCNT nanocomposite, which is capable of delivering about 71 % of its theoretical capacity toward sodium storage (Wang et al. 2013b). An SnO_2-reduced graphene oxide (RGO) nanocomposite with 330 mAh g^{-1} capacities was obtained by Park and coworkers (Wang et al. 2014). In another study conducted by Ahn et al., the Na/SnO_2 cell resulted in huge capacity fading after ten cycles (Park et al. 2014).

The most important focus in the advancement of lithium/sodium batteries is to enhance the lithium/sodium ion and electron transport kinetics in electrodes. To tackle this problem, embedding nanostructured active materials into a three-dimensional conductive porous network is generally suggested (Wang et al. 2013a).

Bacterial cellulose (BC) is an interesting low-cost, nontoxic and biocompatible extrapolymeric carbon material readily produced by various species of bacteria, such as those of the genera *Gluconacetobacter* (formerly *Acetobacter)*, *Agrobacterium*, *Aerobacter*, *Achromobacter, Azotobacter*, *Rhizobium*, *Sarcina* and *Salmonella* (Shoda and Sugano 2005). BC is traditionally used to make the Filipino dessert Nata de coco, served as a gelatinous cube. In stationary culture conditions, these bacteria produce a thick pellicle of cellulose on the surface of the liquid medium. The isolation and purification of bacterial cellulose are relatively simple, not requiring energy- or chemical-intensive processes. Although plant cellulose contains impurities such as lignin, pectin and hemicellulose,

BC is completely pure and highly crystalline (Guo and Catchmark 2012). BC has an ultrafine three-dimensional porous network composed of nanofibers with widths <100 nm, which are smaller than those of plant cellulose. This three-dimensional network provides unique properties to BC including a high tensile strength and high specific surface area. Therefore, BC has been investigated in different fields such as the food industry, medical purposes and additives in the production of paper (Barud et al. 2008; Czaja et al. 2007; Jonas and Farah 1998; Nge et al. 2010). Moreover, BC can also be considered an ideal hydrophilic matrix for metal incorporation to provide additional properties to BC (Shah et al. 2013; Wu et al. 2014; Zhang et al. 2013).

Lignocellulosic materials have gained ample attention because of their availability, low cost and porous structure, resulting in a high surface area of the carbon attained after the pyrolysis process for energy storage devices such as wood (Klijanienko et al. 2008), wheat straw (Li et al. 2010) and coconut husk (Tan et al. 2008). Recently, bacterial cellulose-derived electrically conducting anodic materials and the deposition of active battery components such as binder and electrode separators have shown promising potential in lithium storage capability (Hu et al. 2013; Leijonmarck et al. 2013; Nyström et al. 2009). The pyrolysis procedure compared with hydrothermal carbonization was found to be an easy and effective method for enhancement of surface areas and pore volumes because of the removal of water from cellulose resulting in the contraction of fibers during the process (Hu et al. 2013; Wang et al. 2013a; Wu et al. 2014). Previously, it was shown that the activation process could widen the preformed pores (Huidobro et al. 2001). It was also reported that the pyrolysis process could cause micropore and mesopore formation (Phan et al. 2006). Lee et al. (2013) pyrolyzed BC at 950 °C and physically activated with CO_2 to obtain carbonaceous BC with a graphitic structure.

Herein, we report a simple, unique, low-cost and environmentally benign method to fabricate three-dimensional porous electrode structures, which are compatible with different nanostructured active anode materials. In this study, pyrolyzed bacterial celluloses (PBCs) with a microfibril network structure were used as anode electrodes. We investigated the electrochemical characteristics of microfibril network structure PBCs for NIBs at various heat treatment temperatures and SnO_2 nanoparticle-decorated microfibril network structure PBCs. This is the first report based on the naturally occurring biomaterial BC with a microfibril network structure for sodium ion batteries.

Experimental

Preparation of the bacterial cellulose

Bacterial cellulose (BC) was produced by using *Gluconacetobacter xylinus* (strain BCRC 12334). For BC production, the *G. xylinus* strain was inoculated (2 %, v/v) into 100 ml of Hestrin and Schramm liquid medium (HS) containing 2 % glucose, 0.5 % yeast extract, 0.5 % peptone, 0.27 %. Na_2HPO_4 and 0.15 % citric acid (pH 4.5, Hestrin and Schramm, 1954) in a 500-ml flask and incubated at 30 °C and 50 rpm for 6 days. After incubation, the produced BC samples were washed with distilled water and dried at 60 °C for 4 h.

Synthesis of the materials

The obtained dried bacterial celluloses were pyrolyzed (carbonized) under argon atmosphere at three different temperatures including 500, 750 and 1000 °C. A heating rate of 2 °C min^{-1} was applied and kept for 6 h at the targeted temperature. Materials were described as PBC-500, PBC-750 and PBC-1000 according to their pyrolysis temperatures.

To obtain SnO_2 nanoparticle-decorated PBC (labeled as SnO_2@PBC), SnO_2 nanoparticles were incorporated with BC during the preparation of BCs. First, SnO_2 nanoparticles were synthesized using a hydrothermal method. In a typical synthesis, 2 g $SnCl_4{\cdot}5H_2O$ (Sigma-Aldrich, ≥98 %) was dissolved in 20 ml deionized water. After stirring until complete dissolution, it was heated to 180 °C in a Teflon-lined autoclave (50 ml in capacity) for 20 h. The precipitate was cooled to room temperature naturally and then collected and washed with distilled water and ethanol several times. After drying at 80 °C in a vacuum oven overnight, the final SnO_2 products were obtained. For SnO_2@PBC production, the *G. xylinus* strain was inoculated (2 %, v/v) along with the synthesized SnO_2 nanoparticles (25 mg) into 100 ml of HS medium in a 500-ml flask and incubated at 30 °C and 50 rpm for 6 days. SnO_2@BC nanoparticle composites were

washed with distilled water (Wang et al. 2013a) and dried at 60 °C for 4 h (Scheme 1).

After successful covering of SnO_2 nanoparticles by bacterial cellulose, the resulting products (quoted as SnO_2@PBC) were pyrolyzed at 500 °C for 6 h with a heating rate of 2 °C min^{-1}. Since the calcination temperature above ~600 °C causes thermal reduction of the composite and produces tin (Yu et al. 2013), careful temperature control was maintained during the course of the pyrolysis. After the pyrolysis, the white/yellowish product changed to a black color (Scheme 1).

Characterization of the materials

The phases were characterized by X-ray diffraction. The X-ray powder diffraction patterns of the SnO_2 nanoparticles and SnO_2@PBC were recorded on a Bruker D8 Advance diffractometer (θ–2θ mode, Cu Kα radiation $\lambda = 1.5406$ Å and a linear position-sensitive detector) at a scanning step of 0.02°s^{-1}.

The microstructural and chemical analyses proceeded using a transmission electron microscope (TEM-FEI TECNAI F20 S-TWIN) fitted with a scanning mode and both high-angle annular dark-field (HAADF) detector and EDAX EDS as well as SEM (Philips XL30). The weight ratio between SnO_2 and PBCs was determined by a thermogravimetric analyzer (TGA, PerkinElmer, TGA 4000) between 30 and 700 °C at a heating rate of 10 °C min^{-1} in oxygen atmosphere.

Micro Raman spectra were recorded on a Jobin Yvon LabRam spectrometer (excitation wavelength: 632.8 nm).

Electrochemical characterization

The electrochemical properties of PBC-500, PBC-750, PBC-1000 and SnO_2@PBC materials were evaluated by assembling Swagelok cells in an argon-filled glove box (Innovative Technology, USA). The electrochemical tests were performed in a two-electrode configuration. Sodium metal foils (Sigma-Aldrich) were used as counter and reference electrodes. The working electrodes contained 80 wt% active materials (PBC-500, PBC-750, PBC-1000 and SnO_2@PBC) and 20 wt% super P. The mass loading of the active material was approximately 4 mg cm^{-2}. The electrolyte solution was 1M $NaClO_4$ salt dissolved in a mixture of ethylene carbonate (EC) and propylene carbonate (PC) with a volume ratio of 1:1. The electrochemical performance was tested with a cutoff voltage range from 0.005 to 2 V (vs. Na/Na^+) using a Biologic VMP-3 electrochemical workstation.

Results and discussion

SEM images of the bacterial cellulose (BC) before (Fig. 1a) and after being pyrolyzed at 500, 750 and 1000 °C are shown in Fig. 1b–d, respectively. Although the bacterial cellulose has dense and compact microstructural properties, after the pyrolysis procedure at different temperatures it shows a highly porous network structure constructed by numerous intertwined ultrathin nanofibrils. To further characterize the porous structure of the pyrolyzed bacterial celluloses (PBCs), Brunauer-Emmett-Teller nitrogen adsorption studies were performed. Figure S1 (Electronic supplementary material) depicts the adsorption isotherm of PBC-500, PBC-500 and PBC-1000 (Fig. S1a) and their resulting pore size distributions (Fig. S1b). PBC-500 has a very low surface area of 39.3 m^2 g^{-1} possessing micropores with around 2 nm mean diameter. When the temperature is raised from 500 to 750 and 1000 °C, the surface areas increase dramatically, reaching to 331.3 m^2 g^{-1} and

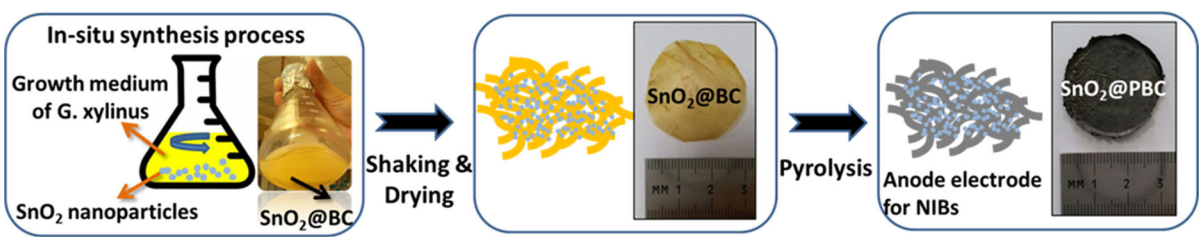

Scheme 1 The synthesis procedure for SnO_2@PBC nanocomposites

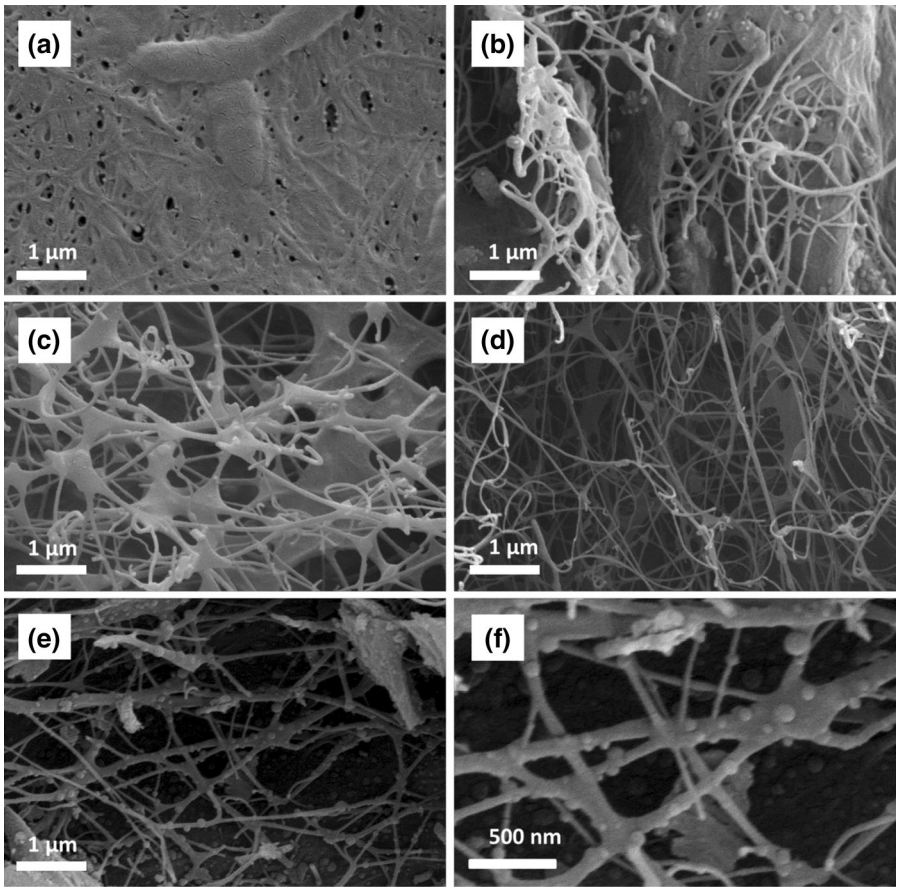

Fig. 1 Morphological characterization of BC, PBCs and SnO_2@PBC composite: SEM images of **a** BC before pyrolysis, **b** PBC-500, **c** PBC-750, **d** PBC-1000, **e** and **f** SnO_2@PBC with different magnifications

662.6 m^2 g^{-1}, respectively. Pyrolysis of the bacterial cellulose was further characterized by Raman spectroscopy. Figure 2a depicts the Raman spectra of the as-synthesized bacterial cellulose and after 750 °C heat treatment under argon atmosphere. The Raman spectrum of the PBC-750 nanocomposite contains the characteristic wide D and G bands around 1360 and 1590 cm^{-1}, respectively, typical for amorphous carbon or disordered graphite, providing defects and a partially disordered nature of the graphitic layers within the PBC. The large intensity value I_D/I_G ($\sim$0.85) indicates the low degree of graphitization of the resulting pyrolyzed bacterial cellulose materials. In contrast, there is no obvious peak observed for the BC spectrum.

The XRD patterns of the pyrolyzed bacterial celluloses treated at 500 °C (PBC-500), SnO_2 nanoparticles and SnO_2@PBC composites are shown in Fig. 2b. Figure 2b shows broad particle size distributions without any aggregation of larger particles for the SnO_2 nanoparticles. The crystallite dimension of SnO_2 nanoparticles along (211) was calculated at around 5 nm by using the Scherrer equation. For the PBC-500, no diffraction peaks corresponding to graphitic carbon were observed in the XRD pattern, meaning that the carbon coating was amorphous. Bacterial cellulose in the presence of SnO_2 nanoparticles was pyrolyzed at 500 °C to eliminate the reduction of SnO_2 to Sn nanoparticles (Fig. 2b). We deduced crystallite dimensions of about 6 nm SnO_2 nanoparticles along the (211) direction after pyrolysis, suggesting that the bacterial culture and temperature treatment do not change the crystallite size and nature of the SnO_2 nanoparticles.

The microstructure of SnO_2 nanoparticles and SnO_2@PBC composite are also analyzed by TEM. The SnO_2 nanoparticles show a rod-like structure with uniform lengths (Fig. 3a). In the SnO_2@PBC composite, SnO_2 particles are successfully surrounded by the bacterial cellulose and dispersed in the bacterial

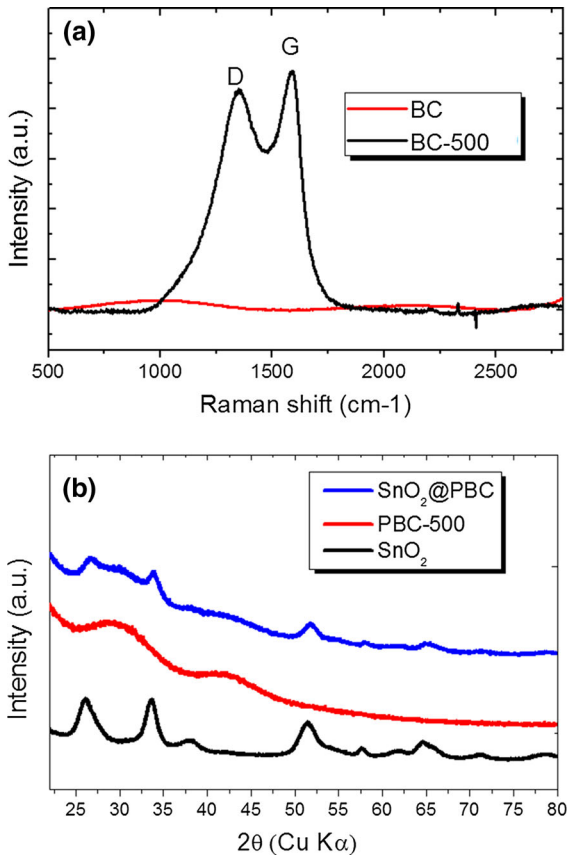

Fig. 2 Structural characterization of samples: **a** Raman spectra of BC and PBC-500, **b** XRD patterns of SnO_2 nanoparticles, PBC-500 and SnO_2@PBC composite

cellulose with some agglomerates. The direct addition of the nanoparticles along with the bacterial culture into the bacterial growth medium allows more interaction between the SnO_2 nanoparticles. During the formation of the in situ coating of SnO_2, PBC keeps its three-dimensional nanofibril porous network structure with obvious SnO_2 nanoparticles (Fig. 1e, f). It was observed that SnO_2 nanoparticles were homogeneously distributed during cellulose production. The reason could be the interaction of oxygen-containing moieties of BC nanofibrils such as hydroxyl groups with the as-synthesized SnO_2 nanoparticles during cellulose production (Barud et al. 2011; Wang et al. 2013a). Indeed, the FT-IR spectrum of the materials (Fig. S2) reveals those oxygenated groups. The wide bands at 3500–3000 cm^{-1} indicate the existence of a large number of hydroxyl groups, which is much higher for the as-synthesized bacterial cellulose than that after being pyrolyzed at 500 °C. The bands at 1640 cm^{-1} can be attributed to the C=O for the BC samples whose intensity decreases upon pyrolysis. Instead, a visible band at 1570 cm^{-1} appears for the PBC samples, which can be attributed to the C=C vibrations, providing the presence of a higher degree of carbonaceous structure.

Production of BC and SnO_2@BC under shaking growth conditions at 50 rpm allowed effective coating of SnO_2 nanoparticles during the cellulose production. Moreover, the shaking incubation conditions led to nanoparticles being well dispersed on the BC bulk ultrafine reticulated structure. For the production of SnO_2@BC nanocomposites, 25 or 50 mg of SnO_2 nanoparticles was incorporated into 100 ml bacterial growth medium. The amount of cellulose production without addition of SnO_2 nanocomposite particles was found as 160 mg dry weight per 100 ml medium after 6 days of incubation; 25 mg of SnO_2 nanoparticles did not affect the growth of *G. xylinus* or the amount of cellulose production. However, the produced cellulose amounts decreased by 30 % (mg dry weight/100 ml medium) with incorporation of 50 mg nanoparticles, respectively, after 6 days. Therefore, the concentration of 25 mg of SnO_2 nanoparticles per 100 ml of medium was used effective for SnO_2@BC nanocomposite production. The weight percent of the SnO_2 in SnO_2@PBC was determined by thermogravimetric analysis (TGA) in O_2 atmosphere indicating around 40 wt% SnO_2 content (Fig. S3 of Electronic supplementary material).

Electrochemical performances of the pyrolyzed-BC electrodes prepared at three different temperatures (PBC-500, PBC-750 and PBC-1000) were first tested in the absence of SnO_2 nanoparticles to understand the impact of the bacterial cellulose matrix. To do so, a comparative electrochemical study had been carried out with three different electrolyte compositions: 1M $NaClO_4$ salt in PC solvent, 1M $NaClO_4$ salt in PC solvent together with FEC additive and 1M $NaClO_4$ salt in a binary mixture of EC:PC as the best solvent formulation and most attractive electrolyte for the development of Na-ion batteries (Ponrouch et al. 2012).

These three electrolytes were examined in Fig. 4 showing the discharge capacity as a function of cycle number for the PBC-500, PBC-750 and PBC-1000. The discharge capacities for all pyrolyzed BCs in the presence of PC electrolyte solution exhibited fast

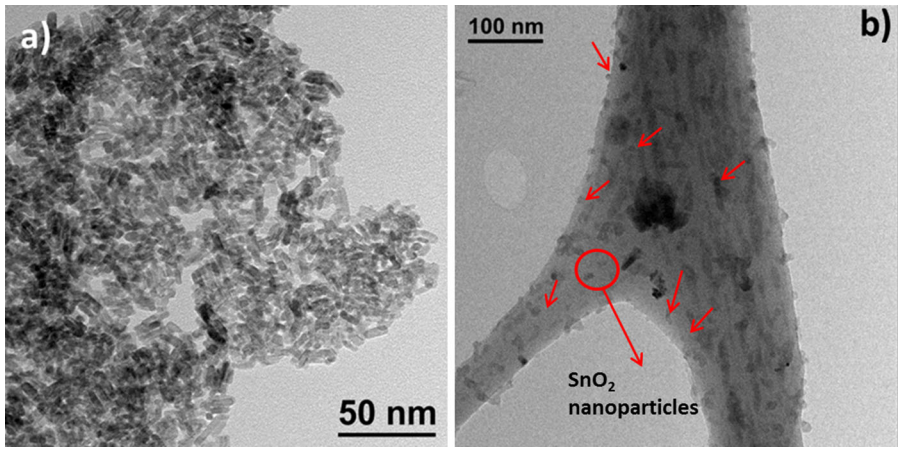

Fig. 3 Morphological characterization of SnO_2 nanoparticles and SnO_2@PBC composite: TEM images of **a** SnO_2 nanoparticles and **b** SnO_2@PBC composite

capacity fading. After adding 5 wt% FEC into the PC solution, the capacity degradation was sufficiently avoided because of the passivation and suppression of the side reactions between the Na metal and electrolyte. The thin passivation layer (SEI surface layer) that formed on the negative electrode was known to be modified by the FEC additive (Komaba et al. 2011a). Conversely, with the binary EC:PC solution containing $NaClO_4$ salt, the PBCs showed better discharge capacity compared to the other electrolytes since the binary EC:PC electrolyte proved to be a much more thermally and electrochemically stable SEI layer with carbonaceous materials (Ponrouch et al. 2012). As can be seen from the voltage versus number of inserted electron curves for all of the combinations at the first cycle (Fig. S4), there was a huge irreversible capacity loss, which was attributed to the presence of the oxygenated group on the surface of the bacterial cellulose matrixes, which was supported above with the FT-IR analysis (Fig. S2), resulting in irreversible Na insertion and SEI formation. To sum up, Fig. 4d shows the discharge capacity of the PBC materials at three different temperatures in the presence of the electrolyte configuration of 1M $NaClO_4$ salt in EC:PC solvent. The first discharge capacities of the PBC-500, PBC-750 and PBC-1000 materials were 194, 451 and 362 mAh g^{-1}, respectively. When the pyrolysis temperature was increased up to 1000 °C, the structure of the materials became more ordered. Since the ordered carbon structure is not suitable for accommodating the larger ionic radius of sodium ions because of the insufficiently large interstitial space, the capacities of the PBC-1000 are much lower than those of PBC-750. We also tested the rate capabilities of the PBC-750 electrode at increasing current rates by gradationally increasing the current rate from 0.1 C up to 10 C (Fig. 4e) and returning the initial current to 0.1 C. At current rates of 0.1, 0.2, 0.5, 1, 2, 5 and 10 C, the reversible discharge capacities of the PBC-750 anode decreased to 161, 134, 88, 61, 44, 25 and 9 mAh g^{-1}, respectively. The PBC-750 recovered almost 100 % of its initial capacity when returning to 0.1 C while presenting a long cycle life and good rate capability.

The sodium storage capacity of the PBC-750 electrode obtained from bacterial cellulose was sufficient, however, to determine the importance of the nanofibril porous structure and compare their performances over other types of cellulose paper (i.e., plant cellulose, commercially available cellulose paper). They were both carbonized at 750 °C for 6 h and tested in the same condition with a constant current rate of 0.1 C in the voltage range of 0.005–2 V (vs. Na/Na^+). The cellulose paper shows (Fig. 4f) smooth and stabile discharge versus Na with a capacity of 50 mAh g^{-1} over 100 cycles; however, the electrochemical performance of the carbon material derived from bacterial cellulose (PBC-750) is almost three times higher than in the cellulose paper.

The number of inserted electron vs. voltage graphs and their discharge capacities are shown in Fig. 5a for the SnO_2@PBC composite at a 0.1 C current density. The first discharge capacity of the SnO_2@PBC

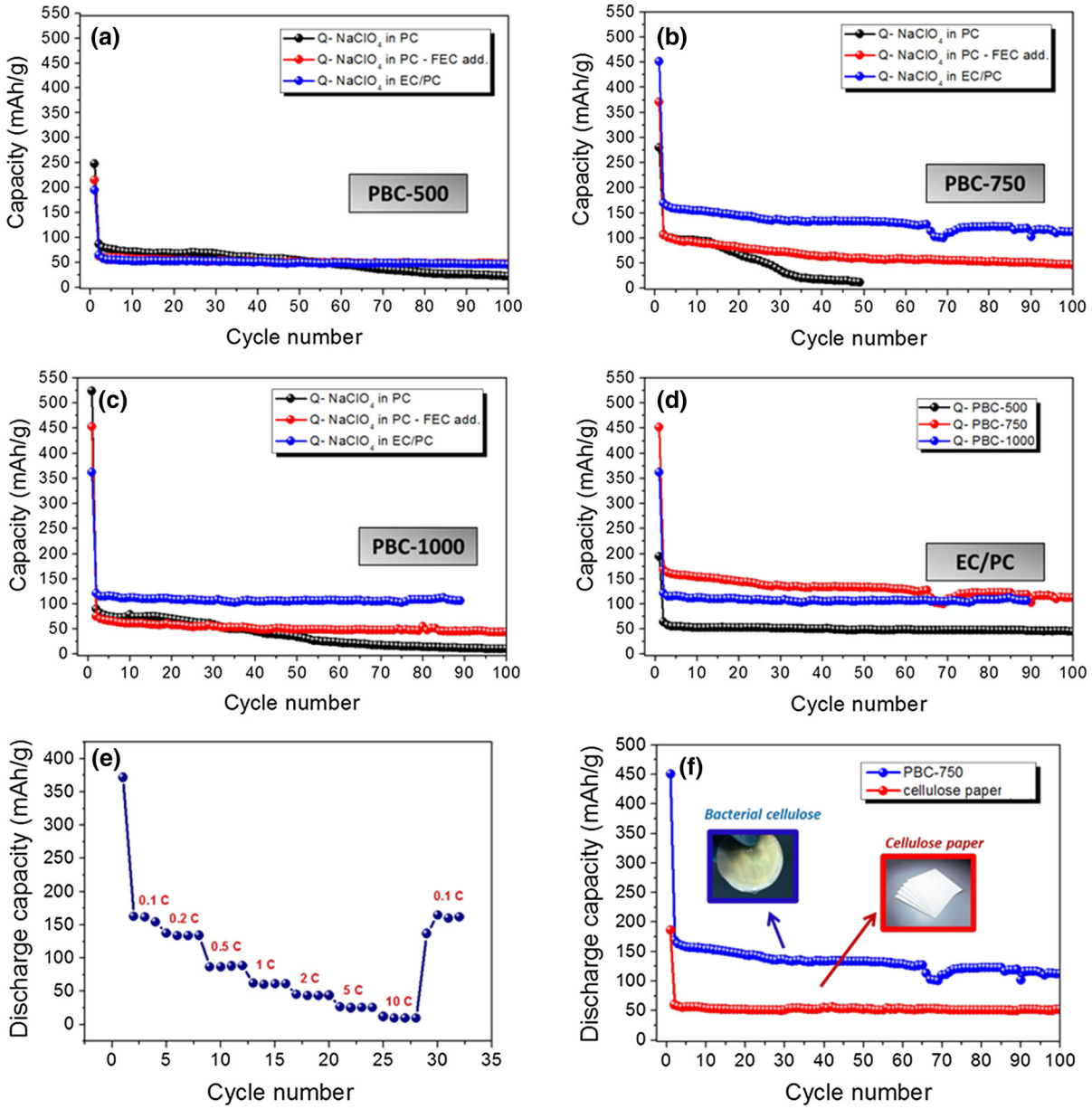

Fig. 4 Cycling performances of PBCs and the rate performances of PBC-750: Effect of electrolytes on the discharge capacity of **a** PBC-500, **b** PBC-750 and **c** PBC-1000 at a C/10 rate, **d** effect of pyrolization temperature on the discharge capacity of PBCs in 1M $NaClO_4$ containing in EC/PC (1:1 wt %) at a C/10 rate in the voltage range of 0.005–2 V (vs. Na/Na^+), **e** rate performances of the PBC-750 electrode at various current rates ranging from 0.1 to 10 C in the voltage range of 0.005–2 V (vs. Na/Na^+) and **f** comparison of PBC-750 and commercially available cellulose paper at a C/10 rate in the voltage range of 0.005–2 V (vs. Na/Na^+)

composite was about 1100 mAh g^{-1}, and they presented a very stable sodiation/desodiation process with a reversible capacity of about 400 mAh g^{-1}. This could be attributed to the SnO_2 nanoparticles being successfully confined in the carbon matrix derived from bacterial cellulose. The SnO_2 nanoparticles, which were surrounded by pyrolyzed carbon, exhibited high conductivity, easy diffusion of Na^+ ions and, most importantly, buffering of the large volumetric expansion during charge/discharge. To the best of our

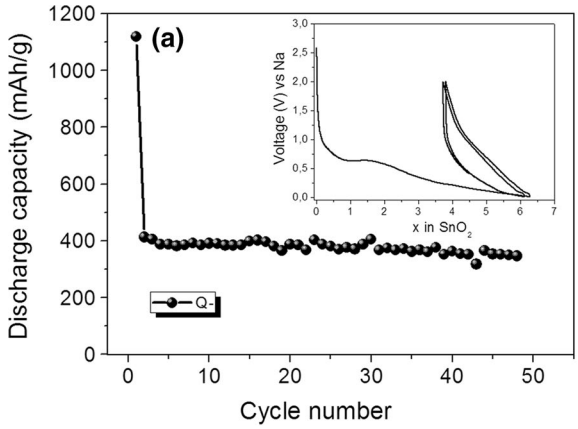

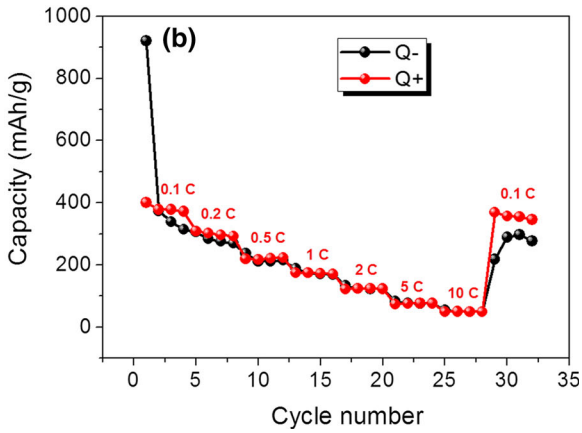

Fig. 5 **a** Cycling and rate performance of the SnO_2@PBC composite: **a** discharge (sodiation) capacity (*inlet* voltage vs. number of inserted electrons) of SnO_2@PBC at a C/10 rate, in the voltage range of 0.005–2 V (vs. Na/Na^+), **b** rate capability of the SnO_2@PBC composite electrode at various current rates from 0.1 to 10 C in the voltage range of 0.005–2 V (vs. Na/Na^+) (*note*: the specific capacity was calculated by using the mass of SnO_2, given in mAh g^{-1})

knowledge, the SnO_2@bacterial cellulose composite has not yet been the subject for an anode material for sodium ion batteries. The specific capacity of SnO_2 alone in the hybrid anode composite, in which both PBC-500 and SnO_2 contributed concurrently to the entire capacity, was estimated by subtracting the contribution of PBC-500. Since the capacity given in Fig. 5a was based on the mass of SnO_2, the entire capacity of the composite was calculated as 160 mAh g^{-1} (400 mAh g^{-1} × 0.4). After deducing the contribution of the PBC-500, which is around 30 mAh g^{-1} (50 mAh g^{-1} × 0.6), the rest of the capacity involvement (130 mAh g^{-1}) was from SnO_2 in the composite. Thus, the contribution of the SnO_2 to the SnO_2@PBC composite depicted in Fig. 5a was calculated as 325 mAh g^{-1} (130 mAh g^{-1}/0.4). Figure 5b shows the rate capability of the SnO_2@PBC composite by gradationally increasing the current rate from 0.1 C up to 10 C and returning to the initial current of 0.1 C. The SnO_2@PBC composite electrode demonstrated a good rate capability. When the electrode was tested at 0.1 C, the capacity was around 400 mAh g^{-1}, which then decreased to 50 mAh g^{-1} when the current rate was increased to 10 C. Conversely, the capacity was recovered when the rate was 0.1 C.

The SnO_2@PBC composite anode was also compared to the SnO_2 + (PBC-500) material for sodium ion batteries at a constant current rate of C/10 (Fig. 6). The SnO_2 + (PBC-500) material was prepared by

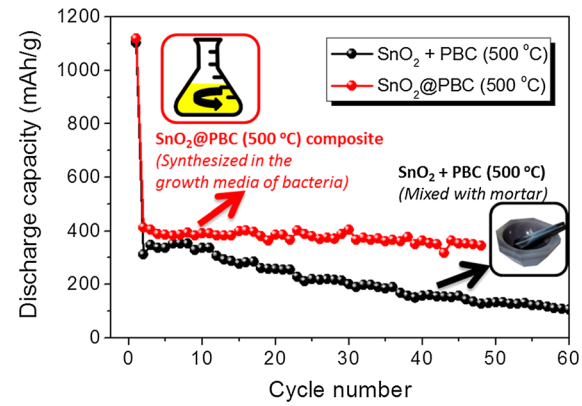

Fig. 6 Capacity retention comparison of SnO_2@PBC composite and SnO_2 + (PBC-500) at a 0.1 C rate, in the voltage range of 0.005–2 V (vs. Na/Na^+) (*note*: in both cases the materials contain 40 wt% SnO_2 and the specific capacities were calculated by using the mass of SnO_2, given in mAh g^{-1})

hand mixing of 40 wt% as-prepared SnO_2 nanoparticles in a mortar together with the as-pyrolyzed bacterial cellulose (PBC-500) in order to clarify the effect of the nanofibril carbon support to the electrochemical performances of the SnO_2@PBC composite. It is clear that the SnO_2@PBC composite, which was prepared by in situ incorporation of the nanoparticles into the growth medium of *G. xylinus*, demonstrates quite good stabile capacity in comparison with the SnO_2 + (PBC-500) material, demonstrating the strong interaction of oxygen-containing moieties of BC nanofibrils with the SnO_2 nanoparticles during

cellulose production, which is not the case for the SnO_2 + (PBC-500) material. As can been seen from Fig. S5, since the SnO_2 + (PBC-500) material was not covered with bacterial cellulose fibrils, their capacity fading was very dramatic because of the huge volume expansion of SnO_2 nanoparticles, which was not compensated by the mechanically mixed PBC-500.

Conclusions

In conclusion, the results of this study show that there is great potential in utilizing bacterial cellulose for the production of nanocomposites as anode materials for sodium-ion batteries. Simultaneous in situ incorporation of SnO_2 nanoparticles with bacterial cellulose producing the *G. xylinus* strain into growth medium for the preparation of an SnO_2@PBC composite enhanced the stabile capacity of the resulting modified BC. The higher number of SnO_2 nanoparticles surrounding regions in the SnO_2@PBC composite exhibited higher conductivity, easy diffusion of Na^+ ions and buffering of a large volumetric expansion during charge/discharge, which could extend the potential applications of BC nanocomposites as anode materials for sodium-ion battery energy storage. Moreover, low-cost scaled-up production of bacterial cellulose for this purpose could be further investigated in future studies.

Acknowledgments The authors appreciate the funding from The Scientific and Technological Research Council of Turkey (TUBITAK contract no. 115M390) and the joint research project between CNRS-TUBITAK (TUBITAK Contract No. 214M272). The *Gluconacetobacter xylinus* strain was a kind gifted from Dr. Cheng Kang Lee (National Taiwan University of Science and Technology, Taiwan). We acknowledge Alice Cassel for the TEM and Ahmet Nazim for the SEM microstructural analyses. Sylvie Grugeon is thanked for helping with the Raman spectroscopy measurements.

Compliance with ethicals standards

Conflict of interest The authors declare no competing financial interest.

References

Alcántara R, Lavela P, Ortiz GF, Tirado JL (2005) Carbon microspheres obtained from resorcinol–formaldehyde as high-capacity electrodes for sodium-ion batteries. Electrochem Solid State Lett 8:A222. doi:10.1149/1.1870612

Antonietti M, Thomas A, Titirici M (2007a) Back in black. J Mater Chem 17:T45–T45

Antonietti M, Thomas A, Titirici M (2007b) Back in black. Lab Chip 7:T45–T45

Barud HS et al (2008) Self-supported silver nanoparticles containing bacterial cellulose membranes. Mater Sci Eng C 28:515–518

Barud HS, Regiani T, Marques RF, Lustri WR, Messaddeq Y, Ribeiro SJ (2011) Antimicrobial bacterial cellulose–silver nanoparticles composite membranes. J Nanomater 2011:10

Cao Y et al (2012) Sodium ion insertion in hollow carbon nanowires for battery applications. Nano Lett 12:3783–3787. doi:10.1021/nl3016957

Czaja WK, Young DJ, Kawecki M, Brown RM (2007) The future prospects of microbial cellulose in biomedical applications. Biomacromolecules 8:1–12

Falco C, Marco-Lozar JP, Salinas-Torres D, Morallon E, Cazorla-Amoros D, Titirici MM, Lozano-Castello D (2013) Tailoring the porosity of chemically activated hydrothermal carbons: influence of the precursor and hydrothermal carbonization temperature. Carbon 62:346–355. doi:10.1016/j.carbon.2013.06.017

Guo J, Catchmark JM (2012) Surface area and porosity of acid hydrolyzed cellulose nanowhiskers and cellulose produced by *Gluconacetobacter xylinus*. Carbohydr Polym 87:1026–1037

Hu L, Liu N, Eskilsson M, Zheng G, McDonough J, Wågberg L, Cui Y (2013) Silicon-conductive nanopaper for Li-ion batteries. Nano Energy 2:138–145

Huidobro A, Pastor AC, Rodríguez-Reinoso F (2001) Preparation of activated carbon cloth from viscous rayon: part IV. Chem Act Carbon 39:389–398. doi:10.1016/S0008-6223(00)00131-7

Jache B, Adelhelm P (2014) Use of graphite as a highly reversible electrode with superior cycle life for sodium-ion batteries by making use of co-intercalation phenomena. Angew Chem 53:10169–10173. doi:10.1002/anie.201403734

Jonas R, Farah LF (1998) Production and application of microbial cellulose. Polym Degrad Stab 59:101–106. doi:10.1016/S0141-3910(97)00197-3

Kim S-W, Seo D-H, Ma X, Ceder G, Kang K (2012) Electrode materials for rechargeable sodium-ion batteries: potential alternatives to current lithium-ion batteries. Adv Energy Mater 2:710–721. doi:10.1002/aenm.201200026

Klijanienko A, Lorenc-Grabowska E, Gryglewicz G (2008) Development of mesoporosity during phosphoric acid activation of wood in steam atmosphere. Bioresour Technol 99:7208–7214

Komaba S, Itabashi T, Kaplan B, Groult H, Kumagai N (2003) Enhancement of Li-ion battery performance of graphite anode by sodium ion as an electrolyte additive. Electrochem Commun 5:962–966. doi:10.1016/j.elecom.2003.09.003

Komaba S, Ishikawa T, Yabuuchi N, Murata W, Ito A, Ohsawa Y (2011a) Fluorinated ethylene carbonate as electrolyte additive for rechargeable Na batteries. ACS Appl Mater Interfaces 3:4165–4168. doi:10.1021/am200973k

Komaba S et al (2011b) Electrochemical na insertion and solid electrolyte interphase for hard-carbon electrodes and application to Na-ion batteries. Adv Funct Mater 21:3859–3867. doi:10.1002/adfm.201100854

Kubo S, White RJ, Tauer K, Titirici M-M (2013) Flexible coral-like carbon nanoarchitectures via a dual block copolymer-latex templating approach. Chem Mater 25:4781–4790. doi:10.1021/cm4029676

Lee K-Y, Qian H, Tay FH, Blaker JJ, Kazarian SG, Bismarck A (2013) Bacterial cellulose as source for activated nanosized carbon for electric double layer capacitors. J Mater Sci 48:367–376

Leijonmarck S, Cornell A, Lindbergh G, Wågberg L (2013) Single-paper flexible Li-ion battery cells through a paper-making process based on nano-fibrillated cellulose. J Mater Chem A 1:4671–4677

Li X, Han C, Chen X, Shi C (2010) Preparation and performance of straw based activated carbon for supercapacitor in non-aqueous electrolytes. Microporous Mesoporous Mater 131:303–309

Nge TT, Nogi M, Yano H, Sugiyama J (2010) Microstructure and mechanical properties of bacterial cellulose/chitosan porous scaffold. Cellulose 17:349–363

Nyström G, Razaq A, Strømme M, Nyholm L, Mihranyan A (2009) Ultrafast all-polymer paper-based batteries. Nano Lett 9:3635–3639

Palomares V, Serras P, Villaluenga I, Hueso KB, Carretero-González J, Rojo T (2012) Na-ion batteries, recent advances and present challenges to become low cost energy storage systems. Energy Environ Sci 5:5884. doi:10.1039/c2ee02781j

Park J et al (2014) Charge–discharge properties of tin dioxide for sodium-ion battery. Mater Res Bull 58:186–189. doi:10.1016/j.materresbull.2014.04.051

Phan NH, Rio S, Faur C, Le Coq L, Le Cloirec P, Nguyen TH (2006) Production of fibrous activated carbons from natural cellulose (jute, coconut) fibers for water treatment applications. Carbon 44:2569–2577. doi:10.1016/j.carbon.2006.05.048

Ponrouch A, Marchante E, Courty M, Tarascon J-M, Palacín MR (2012) In search of an optimized electrolyte for Na-ion batteries. Energy Environ Sci 5:8572. doi:10.1039/c2ee22258b

Ponrouch A, Goñi AR, Palacín MR (2013) High capacity hard carbon anodes for sodium ion batteries in additive free electrolyte. Electrochem Commun 27:85–88. doi:10.1016/j.elecom.2012.10.038

Sangster J (2007) C–Na (carbon–sodium) system. J Phase Equilib Diffus 28:571–579. doi:10.1007/s11669-007-9194-7

Senguttuvan P, Rousse G, Seznec V, Tarascon J-M, Palacín MR (2011) $Na_2Ti_3O_7$: lowest voltage ever reported oxide insertion electrode for sodium ion batteries. Chem Mater 23:4109–4111. doi:10.1021/cm202076g

Sevilla M, Falco C, Titirici M-M, Fuertes AB (2012) High-performance CO_2 sorbents from algae. RSC Adv 2:12792–12797. doi:10.1039/c2ra22552b

Shah N, Ul-Islam M, Khattak WA, Park JK (2013) Overview of bacterial cellulose composites: a multipurpose advanced material. Carbohydr Polym 98:1585–1598

Shoda M, Sugano Y (2005) Recent advances in bacterial cellulose production. Biotechnol Bioprocess Eng 10:1–8

Slater MD, Kim D, Lee E, Johnson CS (2013) Sodium-ion batteries. Adv Funct Mater 23:947–958. doi:10.1002/adfm.201200691

Soorholtz M, White RJ, Zimmermann T, Titirici M-M, Antonietti M, Palkovits R, Schueth F (2013) Direct methane oxidation over Pt-modified nitrogen-doped carbons. Chem Commun 49:240–242. doi:10.1039/c2cc36232e

Stevens DA, Dahn JR (2001) The mechanisms of lithium and sodium insertion in carbon materials. J Electrochem Soc 148:A803–A811. doi:10.1149/1.1379565

Su D, Ahn HJ, Wang G (2013) SnO_2@graphene nanocomposites as anode materials for Na-ion batteries with superior electrochemical performance. Chem Commun 49:3131–3133. doi:10.1039/c3cc40448j

Tan I, Ahmad A, Hameed B (2008) Preparation of activated carbon from coconut husk: optimization study on removal of 2,4,6-trichlorophenol using response surface methodology. J Hazard Mater 153:709–717

Tang K, Fu L, White RJ, Yu L, Titirici M-M, Antonietti M, Maier J (2012) Hollow carbon nanospheres with superior rate capability for sodium-based batteries. Adv Energy Mater 2:873–877. doi:10.1002/aenm.201100691

Wang B et al (2013a) Pyrolyzed bacterial cellulose: a versatile support for lithium ion battery anode materials. Small 9:2399–2404. doi:10.1002/smll.201300692

Wang Y, Su D, Wang C, Wang G (2013b) SnO_2@MWCNT nanocomposite as a high capacity anode material for sodium-ion batteries. Electrochem Commun 29:8–11. doi:10.1016/j.elecom.2013.01.001

Wang Y-X et al (2014) Ultrafine SnO_2 nanoparticle loading onto reduced graphene oxide as anodes for sodium-ion batteries with superior rate and cycling performances. J Mater Chem A 2:529. doi:10.1039/c3ta13592f

Wenzel S, Hara T, Janek J, Adelhelm P (2011) Room-temperature sodium-ion batteries: improving the rate capability of carbon anode materials by templating strategies. Energy Environ Sci 4:3342. doi:10.1039/c1ee01744f

Wu J et al (2014) In situ synthesis of silver-nanoparticles/bacterial cellulose composites for slow-released antimicrobial wound dressing. Carbohydr Polym 102:762–771

Xia X, Dahn JR (2012) Study of the reactivity of Na/Hard carbon with different solvents and electrolytes. J Electrochem Soc 159:A515. doi:10.1149/2.jes111637

Xiong H, Slater MD, Balasubramanian M, Johnson CS, Rajh T (2011) Amorphous TiO_2 nanotube anode for rechargeable sodium ion batteries. J Phys Chem Lett 2:2560–2565. doi:10.1021/jz2012066

Yu L, Cai D, Wang H, Titirici M-M (2013) Hydrothermal synthesis of SnO_2 and SnO_2@C nanorods and their application as anode materials in lithium-ion batteries. RSC Advances 3:17281. doi:10.1039/c3ra42900h

Zhang X, Fang Y, Chen W (2013) Preparation of silver/bacterial cellulose composite membrane and study on its antimicrobial activity. Synth React Inorg Met Org Nano Met Chem 43:907–913

Zhao J et al (2013) Electrochemical and thermal properties of hard carbon-type anodes for Na-ion batteries. J Power Sources 244:752–757. doi:10.1016/j.jpowsour.2013.06.109